

Cite this: *RSC Adv.*, 2013, **3**, 21604

## A study of DNA design dependency of segmented DNA-induced gold nanoparticle aggregation towards versatile bioassay development†

Yen Nee Tan, Kwai Han Lee‡ and Xiaodi Su\*

DNA-decorated gold nanoparticles (AuNPs) are important sensing probes for designing versatile assays for detecting DNA hybridization, DNA binders and DNA associated biological processes. In this study, we report DNA design rules for a pair of segmented DNA-conjugated AuNPs that can undergo “transient” aggregation due to cooperative base-pairing force of sticky ends on DNA and salt screening. A wildtype estrogen receptor response element (ERE) was used as a model DNA which is segmented into two half-sites, each carrying a complementary sticky end and a half-site DNA, were conjugated onto AuNPs to form two sets of complementary DNA–AuNPs conjugates. A number of DNA design parameters are studied for their effects on the aggregation kinetics, namely DNA conformation (*i.e.*, mixed structure of ssDNA and dsDNA), number of sticky-ends bases, spacer length, as well as the symmetrical and asymmetrical interplay between the complementary set of segmented DNA–AuNPs conjugates. Firstly, we found that dsDNA serves as a more effective spacer than ssDNA in preventing base coordination of the nucleotides to the AuNPs surface due to its rigidity that in turn helps to improve the accessibility of sticky-ends for faster aggregation. Secondly, base-pairing force in facilitating the salt-induced AuNPs aggregation is tunable by the number of sticky-ends, which is closely related to the length and structural composition of the DNA spacer. Thirdly, symmetrically spaced sticky-ends enable quicker non-crosslinking aggregation than the asymmetrical combination due to their closer initial interparticle distance. Based on the optimized DNA design, we appended the efficient aggregation that leads to transient formation of a full ERE sequence for detecting estrogen receptor  $\beta$  (ER  $\beta$ ) by exploiting protein binding retarded particle aggregation. With a competition assay, binding affinity of ER $\beta$  to different DNA sequences can be easily screened using a single set of complementary segmented DNA–AuNPs probes. The DNA design dependency of the DNA–AuNPs aggregation studied herein has enabled potential applications for rapid and highly specific DNA-binding protein detection, which could be extended to detect a wide range of DNA binders and its related biological processes.

Received 21st May 2013  
Accepted 4th September 2013

DOI: 10.1039/c3ra44661a

[www.rsc.org/advances](http://www.rsc.org/advances)

### Introduction

DNA-conjugated gold nanoparticles (AuNPs) are important sensing elements for detecting DNA,<sup>1–4</sup> DNA binders (*e.g.*, drug, protein and metal ions)<sup>5–10</sup> and DNA-related biological processes (*e.g.*, gene transcription, enzymatic cleavage and DNA methylation).<sup>11–15</sup> AuNPs in those systems provide the essential optical readout because the color and UV-visible (UV-vis) spectrum of the colloidal gold solution are determined by the assembly

(aggregation) or disassembly (dispersion) status of the nanoparticles that is largely manipulated by DNA-related biomolecular interactions.<sup>1,16</sup> Eyeing on this attractive interparticle distance-dependent optical property of AuNPs for various bioassay developments,<sup>17,18</sup> there have been profound works on the design of decorating DNA (including DNA spacer and recognition sequences)<sup>19–24</sup> caps on AuNPs surface and the design of non-conjugated linker DNA<sup>5,16,25–27</sup> to control the nanoparticle assembly processes from slow to high rate (see Table 1).


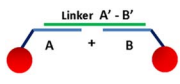
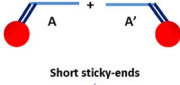
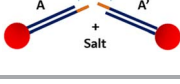
In a typical system (denoted as scheme I in Table 1), two sets of AuNPs separately functionalized with decorating DNAs, containing complementary DNA sequences (A and A') and a single-stranded DNA (ssDNA) spacer, are mixed together to form polymeric aggregates of AuNPs with DNA-duplex interconnects through direct conjugate–conjugate hybridization, detectable as red-to-purple color change and red shift of the localized surface plasmon resonance (LSPR) peak. However, this type of interparticle cross-linking method is reported to be

*Institute of Material Research and Engineering, A\*STAR (Agency for Science, Technology and Research), 3 Research Link, Singapore 117602. E-mail: xd-su@imre.a-star.edu.sg*

† Electronic supplementary information (ESI) available: Fig. S1 for DNA structural spacer design (*i.e.*, 16 + 3-st) and Table S1 for DNA sequences used in the study. See DOI: 10.1039/c3ra44661a

‡ Nanyang Technological University, Singapore. Conducted this research when she was an attachment student with the Institute of Materials Research and Engineering, Singapore.

**Table 1** Scheme and aggregation principle of DNA-conjugated AuNPs

| Scheme | DNA–AuNPs conjugates  | Aggregation Principle   | Type                                   |
|--------|---|---|--|
| I      |  | ssDNA spacer-facilitated direct conjugate-conjugate hybridization <sup>28</sup>   | Interparticle crosslinking aggregation |
| II     |  | ssDNA spacer-facilitated sandwich hybridization with DNA linker <sup>25</sup>   | Interparticle crosslinking aggregation |
| III    |  | dsDNA spacer-facilitated direct conjugate-conjugate hybridization <sup>24</sup>   | Interparticle crosslinking aggregation |
| IV     |  | Synergetic 'transient' base-pairing and salt screening driven by <i>London-van der Waals</i> attractive force <sup>11</sup> | Non-crosslinking aggregation           |

Slow  
Rate of Aggregation  
Fast

very slow (at least 12 hours) for aggregation/color change to be observable,<sup>28</sup> although ssDNA spacers are often introduced between the conjugated site on AuNPs and the recognition sequence. Mirkin and coworkers have creatively utilized such DNA–AuNPs aggregates (pre-formed) for colorimetric screening of endonuclease activity and inhibition.<sup>14</sup> In an alternative scheme, particle aggregation through sandwich hybridization with a DNA linker is reported for colorimetric DNA detection (scheme II in Table 1).<sup>25</sup> In this assay design, two sets of AuNPs are functionalized with two different ssDNA probes, *i.e.*, A and B, respectively. The presence of a target DNA (or DNA linker) that contains the complementary sequence (A' and B') will crosslink the particles through multiple A–A' and B–B' hybridization links on each particle, leading to detectable solution color changes. Recently, this investigation has been refined into the development of highly-organized DNA–AuNP assemblies from two-dimensional structures to three-dimensional crystalline assemblies based on scheme II.<sup>25,27,29–31</sup> For example, Park *et al.*<sup>27</sup> reported the control of DNA-directed AuNPs assembled crystalline structures between face-centered-cubic (fcc) and body-centered-cubic (bcc) unit cells by manipulating the DNA-linker design and thermal condition of the crystallization process. An fcc crystal is found to form ten times quicker than a bcc crystal,<sup>31</sup> which set an interesting point of our investigation for biosensing purposes. All-in-all, these works are pointing towards a broad field of exploration for different types of aggregation-based AuNPs assays *via* proper design of DNA–AuNPs conjugates.

DNA-directed AuNPs assembly is now known to be tunable by optimizing the linker DNA's structural composition (*e.g.*, either pure ssDNA or pre-annealed DNA with overhangs and/or gap),<sup>5,16,25,26</sup> decorating DNA's length,<sup>11,20</sup> DNA spacer's sequence and conformation,<sup>23,24,32</sup> as well as particles aggregation (*e.g.*, crosslinking and/or non-crosslinking) mechanisms.<sup>8,14,18,33–35</sup> For sensing purposes, the design of DNA spacer between the conjugated site on AuNPs and the recognition sequence for hybridization plays an important role in reducing the steric crowding<sup>23</sup> and increasing the accessibility of the nucleotide bases for base-pairing.<sup>24</sup> In both assay schemes I and II, ssDNA fragment (*i.e.*, poly T or poly A)<sup>10,20,22,23</sup> are often used as a spacer

to prevent the recognition DNA sequence from adsorbing onto the AuNP surface through base coordination binding that will impede the hybridization with its target DNA strand. Lately, Gang's group demonstrated the use of double-stranded DNA (dsDNA) as a spacer to speed up the AuNPs aggregation *via* the direct conjugate–conjugate hybridization (scheme III).<sup>24</sup> They attributed the observed 2-fold kinetic enhancement to the added rigidity of the dsDNA spacer, leading to the extension of DNA recognition sequences for more efficient target hybridization on AuNPs.

More recently, driven by the demand of a rapid assay for detecting DNA binding protein and inspired by the versatile DNA-directed AuNPs assembly, we developed a protein sensing assay (for estrogen receptor  $\alpha$ , ER $\alpha$ ) exploiting non-crosslinking aggregation through 'transient' base-pairing and salt/charge screening mechanism.<sup>11</sup> Typically two sets of DNA-conjugated AuNPs were involved (scheme IV in Table 1), each of the decorating DNA containing a half site of the protein binding element (denoted as the segmented DNA) that consist of a dsDNA fragment (being considered as a spacer) and a short sticky-end. In this aggregation-based AuNPs assay, the short sticky-ends of the two segments are complementary despite they are not stable at room temperature. We have proven that the transient base-pairing is the key driving force that initiates the salt-induced aggregation of AuNPs while the binding of specific protein analyte to its recognized 'complete' DNA sequences retard the aggregation through sequence-specific protein–DNA recognition.

Herein, to better understand the mechanism of this assay design for more efficient detection of DNA-binding protein, we systematically studied the efficiency of the transient AuNPs assembly of the complementary set of segmented conjugates, with various design parameters of the decorating DNA. These parameters include (1) mixed structure of DNA spacer (ssDNA and dsDNA), (2) length of dsDNA spacer, (3) number of sticky-end bases, as well as the (4) symmetrical and asymmetrical interplay between the complementary set of segmented DNA–AuNPs conjugates. Estrogen receptor  $\beta$  (ER $\beta$ ) was used as a model protein. With the optimal design parameters (*i.e.*, a longer dsDNA portion in the spacer of 16-bp, a 3-base sticky-end, and a total length of 35-bp with symmetrical dsDNA

spacers appended on each AuNPs probe), the segmented DNA–AuNPs assay was amended for screening of ER $\beta$  binding specificity to different DNA sequences using a competitive assay arrangement. With this competitive assay, ER $\beta$ –DNA specificity is determined for a large number of DNA without the need of AuNPs conjugations for every tested DNA sequences. This assay design offers a highly convenient yet specific and fast alternative for studying protein–DNA binding interactions, which could be extended to detect a wide range of DNA binders and its related biological processes.

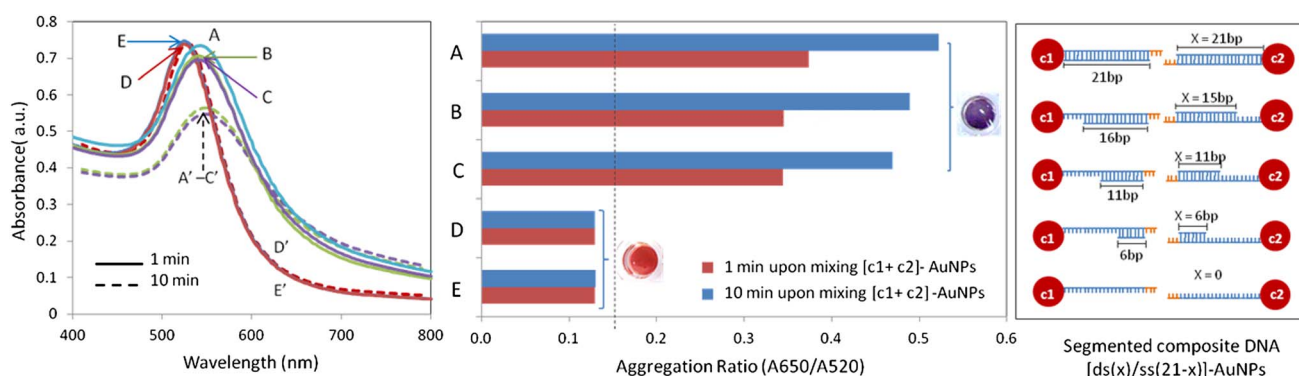
## Results and discussion

### Structural effects of DNA spacer composition (ssDNA and/or dsDNA) on ‘transient’ base-pairing and salt-induced AuNPs aggregation

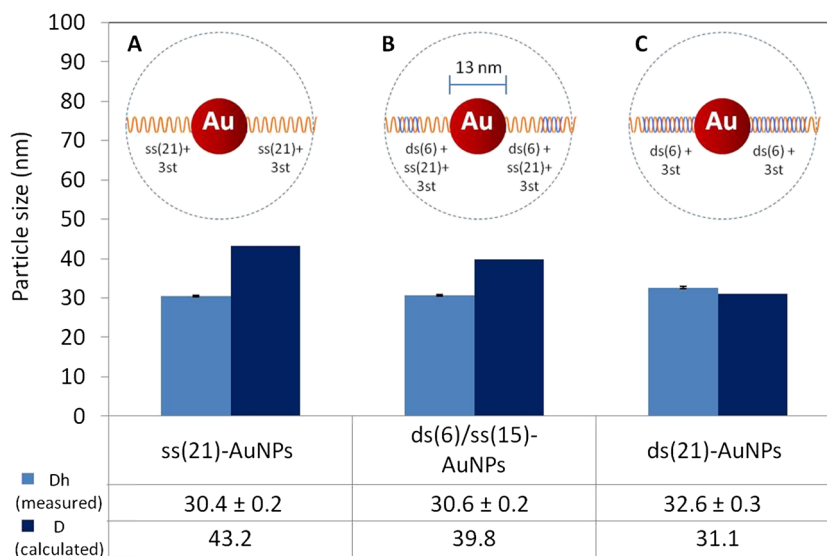
We first investigate the conformation of DNA spacer on the non-crosslinking aggregation of AuNPs through the ‘transient’ base-pairing mechanism of short complementary sticky-ends (st) in salt solution. A 45 mer model DNA sequence (refer to Table S1†) containing a perfect core sequence for estrogen receptor ( $\alpha$  and  $\beta$ ) at the center was segmented into two half-sites (c1 and c2). The c1 and c2 were conjugated onto two set of AuNPs, respectively. Schematic diagram in Fig. 1 (right) shows the details of the segmented DNA–AuNPs conjugates design, DNA<sub>(y+3-st)</sub>–[ds(x)/ss(y–x)]–AuNPs, where  $x$  denotes as the length of dsDNA portion in the composite decorating spacer;  $y$  denotes as the total length of spacer connected to a 3-base sticky-ends (3-st). Particularly, DNA structures (21 + 3-st) containing different composition of ssDNA and dsDNA (*i.e.*,  $x = 0, 6, 11, 16$ , and 21-bp) are studied and the UV-vis spectrum of each complementary set of mixture conjugates (c1–AuNPs and c2–AuNPs at 1 : 1 molar ratio) with different DNA spacer composition was obtained upon addition of 25 mM KCl in 0.1 M PBS buffer solution (Fig. 1, left). Upon aggregation, the LSPR peak of well-dispersed AuNPs at 525 nm decreases and shifts to a longer wavelength (*e.g.*, 650 nm). The UV-vis absorbance ratio of 650 nm to 525 nm (*i.e.*,  $A_{650}/A_{525}$ ) thus indicates the degree of AuNPs aggregation ( $R$ ). Typically for red color dispersed AuNPs, the ratio is lower than

0.15, and  $R$  starts to increase as the aggregation proceeds (solution turning to purple/blue color). The calculated aggregation degree or  $R$  ratio in Fig. 1 (middle) portrays a high dependency of base-pairing efficiency on the rigidity of DNA spacer (*i.e.*, length of dsDNA portion) between the AuNPs and 3-base sticky-ends. As the ssDNA gap between AuNPs and dsDNA portion increases with shortened dsDNA portion, the  $R$  ratio decreases, *i.e.*,  $R = 0.12, 0.47$ , and  $0.52$  when  $x = 6, 11$  and 21, at  $t = 10$  min upon mixing the complementary conjugates. This indicates a decrement in the accessibility of the sticky-ends heading the dsDNA portion. Extremity occurs when the length of dsDNA portion is shorter than 11 base-pairs. For example, [ds(6)/ss(15)]DNA–AuNPs mixtures ( $x = 6$ , Fig. 1D) exhibits the same degree of aggregation as the complementary mixture of the [ss(21)]DNA–AuNPs ( $x = 0$ , Fig. 1E) where both samples display stable red color solution and recorded an aggregation ratio of  $R = 0.12$ . This is in agreement with the previous studies that pure ssDNA hybridization induced cross-linked assembly of AuNPs usually takes very long (*i.e.*, 8 hours) to present a small redshift of LSPR peak due to the inefficiency of interparticle base-pairing.<sup>24</sup> For our case, non-crosslinking AuNPs aggregation due to the transient base-pairing of short DNA sticky-ends and salt screening could facilitate immediate redshift of LSPR peak from 525 to 545 nm, and obvious color change from red to purple upon mixing the complementary sets of AuNPs conjugates, especially when there are sufficient length of dsDNA spacer (for  $x = 21, 16$  and 11, Fig. 1A–C). This trend is also observed in the system when another set of DNA structural spacer design (*i.e.*, 16 + 3-st) was used in our study (Fig. S1, ESI†), further confirm the correlation between DNA rigidity and aggregation efficiency of the complementary segmented DNA–AuNPs mixture.

To gain further insight into the correlation between the conformation of the decorating DNA on AuNPs and the corresponding base-pairing tendency of the 3-base sticky-ends, hydrodynamic diameter ( $D_h$ ) of three segmented DNA<sub>(21+3-st)</sub>[ds( $x$ )/ss(21– $x$ )]–AuNPs, containing either pure ssDNA ( $x = 0$ ), pure dsDNA ( $x = 21$ ), or mixed structure of dsDNA/ssDNA ( $x = 6$ ) spacer were measured using dynamic light scattering (DLS) (Fig. 2). Results were compared with the calculated diameter of



**Fig. 1** Spacer effect as a function of DNA conformation on AuNPs aggregation efficiency. UV-vis spectra (left) and the calculated aggregation ratio (middle) upon mixing complementary set of DNA<sub>(21+3-st)</sub>–AuNPs conjugates (*i.e.*, c1–AuNPs and c2–AuNPs at 1 : 1 molar ratio) with composite DNA spacer containing varying length of dsDNA ( $x$ ) and ssDNA (21 –  $x$ ), in 25 mM KCl and 0.1 M PBS buffer solution.  $x = 21, 16, 11, 6$ , and 0 for samples A, B, C, D, E, respectively. (Right) schematic illustrations of the corresponding design of DNA spacers conjugated on AuNPs (only one DNA strand on each AuNP is shown from clarity and not drawn to the scale).



**Fig. 2** DLS measurement of hydrodynamic diameter and calculated size of DNA<sub>(21+3-st)</sub>[ds(x)/ss(21 - x)]-AuNPs conjugates from the sum of average AuNPs diameter (13 nm), DNA spacer of different composition: (A) 21 mer ssDNA, (B) ds(6)/ss(15)DNA, (C) 21-bp dsDNA, and 3-base sticky-ends (3-st). The contour length of a fully-stretched ssDNA is calculated based on 0.63 nm per base while dsDNA is based on 0.34 nm per base pair.<sup>36</sup>

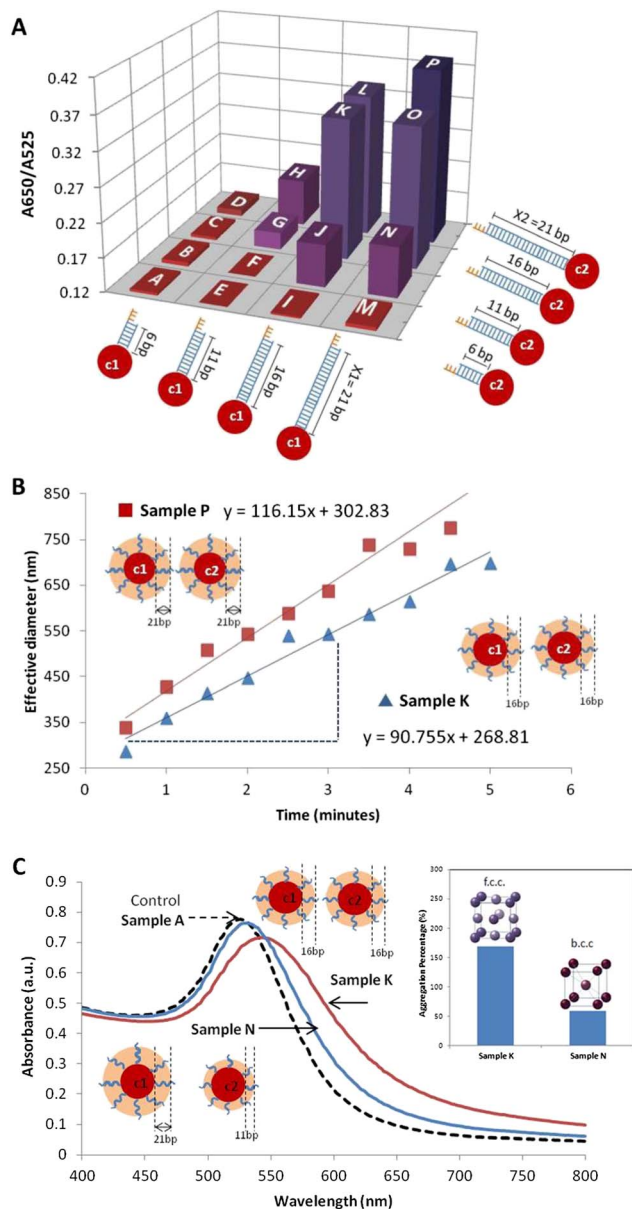
respective AuNPs conjugates from the sum of average AuNPs diameter (13 nm) and the DNA spacer length of different ss- and dsDNA composition and the 3-base sticky-ends. The contour length of a fully-stretched ssDNA is calculated based on 0.63 nm per base while dsDNA is based on 0.34 nm per base pair.<sup>36</sup> Based on this simplified calculation, the [ss(21)]DNA-AuNPs (consist of 13 nm AuNPs, 21 mer ssDNA spacer, and 3-base sticky-end) shall have an estimated  $D_h$  of 43.2 nm, yet its measured hydrodynamic diameter is only  $30.4 \pm 0.2$  nm (Fig. 2A). This suggests that ssDNA has a high tendency to bend and lie onto the AuNPs surface. A discrepancy between the measured hydrodynamic diameter of [ds(6)/ss(15)]DNA-AuNPs ( $D_h$  of  $30.6 \pm 0.2$  nm) and its calculated diameter of 39.8 nm is also observed for the mixed structure DNA spacer containing longer ssDNA portion than the less flexible dsDNA counterpart. The longer portion of ssDNA in the spacer would shorten the overall extension of the short sticky-end towards solution, which does not favor the base-pairing event. This explain why the complementary mixtures of [ds(6)/ss(15)]DNA-AuNPs is not responsive to the transient base-pairing and salt-induced aggregation as shown in Fig. 1D. On the other hand, when dsDNA is used as the only component of the spacer, the measured hydrodynamic diameter of [ds(21)]DNA-AuNPs ( $D_h = 32.6 \pm 0.3$  nm) is very close to its calculated size of 31.1 nm (Fig. 2C). This finding, together with the previous aggregation results (Fig. 1A–C), suggests a favorable extension of the short sticky-ends by the rigid dsDNA spacer that could facilitate efficient transient base-pairing for instant aggregation in salt solution. The efficiency of dsDNA as spacer for improving transient base pairing increases as the dsDNA component in the spacer segments increases. In other words, with increasing rigidity effect and decreasing base coordination of the nucleotide to the AuNPs surface, dsDNA component in a spacer plays a role for effective DNA-based assembly of AuNPs *via* transient base-pairing and

non-crosslinking aggregation mechanism as demonstrated in this study.

#### Length effects of dsDNA spacer on complementary segmented conjugates and their symmetrical and asymmetrical interplay on AuNPs aggregation

By manipulating the composition of the DNA spacer, we have shown that the rigidity of DNA spacer (*i.e.*, a substantial portion of dsDNA over ssDNA) plays a critical role in AuNPs aggregates driven by the transient base-pairing of the short overhangs in salt solution. In this session, we further assess the length effects of DNA spacer with pure dsDNA of 6, 11, 16, and 21-bp on the transient base-pairing to the AuNPs aggregation kinetics, and study the symmetric and asymmetric interplay from a mixture of complementary segmented DNA-AuNPs conjugates with either the same or different length of dsDNA spacer. The 3-st overhang is used in this study. Fig. 3A shows the aggregation degree of AuNPs samples mixed at various combination of c1 [ds( $x_1$ )]-AuNPs and c2[ds( $x_2$ )]-AuNPs, which contains different length ( $x = 6, 11, 16$ , and 21-bp) of dsDNA spacer, at 1 : 1 molar ratio in 25 mM KCl and 0.1 M PBS. It was found that the aggregation degree is largely determined by the total length ( $x_1 + x_2$ ) of the dsDNA spacer in the complementary sets of conjugates. For example, sample P ( $x_1 + x_2 = 42$ ) shows the largest aggregation followed by samples O/L ( $x_1 + x_2 = 37$ ) and sample K ( $x_1 + x_2 = 32$ ). For a fixed total length (*i.e.*,  $x_1 + x_2 = 27$ ), samples G/J with a (11 + 16) combination give detectable aggregation, but not samples D/M with a (6 + 21) combination. This suggests a threshold of 11-bp in any of the conjugate that is essential to extend the short sticky-ends from the AuNPs surface for efficient base-pairing. Similarly, for a fixed length of  $x_1 + x_2 = 32$ , sample K with the (16 + 16) combination aggregates more significantly than the (11 + 21) combination for samples N/H,





**Fig. 3** Length effects of dsDNA spacer and their symmetrical and asymmetrical interplay on AuNPs aggregation efficiency. (A) Aggregation ratio for samples mixed at various combination of c1[ds( $x_1$ )]-AuNPs and c2 [ds( $x_2$ )]-AuNPs, that contains different length ( $x = 6, 11, 16$ , and  $21$  bp) of dsDNA spacer connecting with a 3-base sticky-end, at  $1 : 1$  molar ratio in  $25$  mM KCl and  $0.1$  M PBS buffer. (B) Aggregation kinetics of symmetrical combination of dsDNA spacer length for sample P ( $21 + 21$ ) and K ( $16 + 16$ ) based on DLS measurement of their aggregate sizes over time. (C) UV-visible spectra of the complementary mixture of segmented (c1 + c2)[ds( $x_1 + x_2$ )]DNA-AuNPs (total spacer length of  $x_1 + x_2 = 32$  bp) with asymmetrical combination of  $21 + 11$  for sample N compare with the symmetrical combination of  $16 + 16$  for sample K. A non-aggregating mixture of sample A ( $6 + 6$ ) was used as control. Inset shows the calculated aggregation percentage  $R^* = (R_{\text{competitor}} - 0.12)/0.12$ , with  $0.12$  as the benchmark  $A_{650}/A_{526}$  ratio for a non-aggregating mixture (sample A).

which further indicates the importance of adequate dsDNA length of both sets of conjugates in promoting the aggregation. This also explains why the samples (e.g., sample A to E) with either  $x_1$  or  $x_2 < 11$  show no observable aggregation with  $R < 0.15$ .

Arising from the mix-and-match experiments above, the symmetrical effect of the segmented dsDNA-conjugated AuNPs mixture (for sample A, F, K and P, where the length of each spacer are identical *i.e.*,  $x_1 = x_2$ ) on the base-pairing and salt-induced aggregation was further investigated here. Particularly, DLS was used to monitor the growth rate in term of their aggregate size change for sample K (*i.e.*,  $16 + 16$  combination) and sample P (*i.e.*,  $21 + 21$  combination) as a function of time upon mixing. Prior to the mixing experiment, the hydrodynamic diameter of c1[ds( $16$ )]-AuNPs is recorded as  $31.4 \pm 0.2$  nm while that for c1[ds( $21$ )]-AuNPs is  $32.6 \pm 0.3$  nm. As early as half a minute mixing, about 10-fold increment in particle size, *i.e.*,  $285.8$  nm for sample K and  $338.7$  nm for sample P, was observed. The aggregation kinetic over 5 minutes (Fig. 3B) shows that sample P exhibited a faster aggregate growth rate of  $116.2$  nm  $\text{min}^{-1}$  than that of sample K, *i.e.*,  $90.8$  nm  $\text{min}^{-1}$ . As reported in the previous section and in agreement with Maye's work,<sup>24</sup> the length of rigid dsDNA spacers is positively related to hydrodynamic diameter of the DNA-conjugated AuNPs. The rigid dsDNA spacer is presumably extending the sticky-ends away from the AuNPs surface to reduce its single base coordination to the AuNPs surface. As the hydrodynamic diameter of DNA-AuNPs conjugates increases with the length of dsDNA spacer, this expands the distance between the sticky-ends due to surface curvature of AuNPs, thus improving the particle aggregation efficiency. This explains why samples A (*i.e.*,  $6 + 6$  combination) and F (*i.e.*,  $11 + 11$  combination) with short dsDNA spacers reported no aggregation tendency due to the low accessibility of the sticky-ends for base-pairing. It is also worth notice that the interparticle distance between DNA-assembled AuNPs by the crosslinking mechanism is reported to be larger as the DNA linkers increases in length.<sup>27</sup> Ideally, assembly with larger initial interparticle distance upon the base-pairing is supposed to have a lower degree of aggregation upon base-pairing. However, our results suggest the other way in which the longer the dsDNA spacer, the larger the degree of AuNPs aggregation is observed with larger  $R$  value. This observation indicates the dominance of dsDNA length in enhancing the transient base-pairing through non-crosslinking mechanism. The transiency of nanoparticles aggregation is attributed to the perturbation of KCl screening and the weak base-pairing between the short sticky-ends heading the dsDNA spacer.

In addition to the symmetrical effect of spacer length as discussed earlier, it is observed that the *asymmetrical* combination of spacer length for the complementary c1 + c2[ds( $x_1 + x_2$ )]-AuNPs that produce the same total length of dsDNA as the symmetrical combination, *e.g.*, samples K ( $16 + 16$ ) and N/H ( $21 + 11$ ), exhibited different extent of AuNPs aggregation. Fig. 3C shows the UV-vis spectra and the calculated aggregation percentage (*i.e.*,  $R^* = (R - 0.12)/0.12$ , with  $0.12$  as the benchmark of  $A_{650}/A_{526}$  ratio for a non-aggregating mixture) of samples K and N, respectively. It was noticed that sample K with symmetrical combination of spacer length ( $16 + 16$ ) displays an aggregation of about 3 folds more intensive than the asymmetrical mixture of sample N with ( $21 + 11$ ) combination. The symmetry of the DNA-AuNPs has been reported as one of the controlling factor of the DNA-linked AuNPs crystalline

structure.<sup>27</sup> The different crystalline structures of the AuNPs assembly having different atomic packing factor, in turn affects the initial interparticle distance prior to KCl charge screening. The symmetrical combination of c1 + c2[ds(16 + 16)]-AuNPs (K) presumably forms a close-packed face-centered cubic structure (face atomic packing factor for fcc = 0.74) whereas the asymmetrical combination of c1 + c2[ds(21 + 11)]-AuNPs (N) formed a non-close-packed body-centered cubic structure (atomic packing factor for bcc = 0.68). The difference in the initial interparticle distance governed by the crystalline structure renders a significant difference in the aggregation upon charge screening. Therefore, the transient symmetrical DNA-assembly of AuNPs can induce larger degree of aggregation by charge screening destabilization due to its shorter initial interparticle distance.

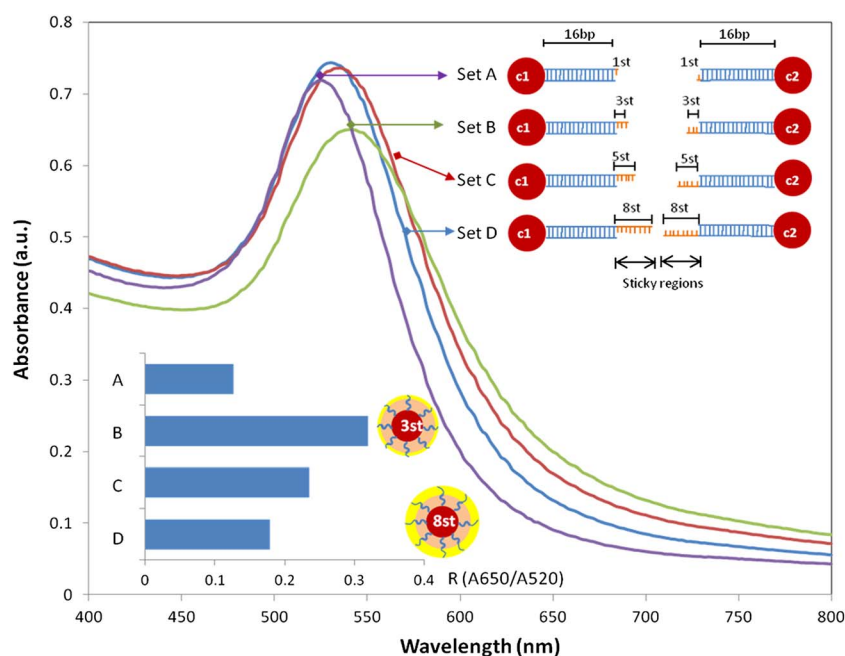
### Length effects of sticky-ends heading the dsDNA spacer on transient base-pairing and non-crosslinking AuNPs aggregation

Despite of the favorable extension of sticky-ends by the rigid dsDNA spacer for efficient random assembly of the symmetrical segmented DNA-AuNPs conjugates, the number of sticky-end bases that governs the base-pairing affinity to bring forward AuNPs in close vicinity for charge screening is another key driving force for non-crosslinking aggregation. As shown in Fig. 4, four complementary sets of segmented c1 + c2[ds(16) + (z) st]-AuNPs conjugates with a fixed length of 16 mer dsDNA spacer for each conjugate and varying base number of sticky-ends (*i.e.*,  $z = 1, 3, 5$  and 8-st), were studied. It is observed that when sticky region  $z = 1$ -st, there is no aggregation occurred

after mixing despite having the same extended length of rigid dsDNA spacer under the designated salt condition. The hybridization tendency of the single-base at the sticky-end is deemed too low to induce adequate driving force bringing the AuNPs close to each other, whereas DNA-AuNPs with 3 bases in its sticky-ends region is found as the most aggregated mixture. As  $z$  increases from 3 to 5 and 8-st, the degree of particle aggregation decreases (*i.e.*,  $R$  value decreases). With the same DNA-capping shell thickness of the dsDNA spacer, the system is similarized to the ssDNA-conjugated onto a larger AuNPs. As the flexible ssDNA sticky-ends increases in length, the dynamic bending and random coiled structure of the ssDNA could impede the rate of base-pairing. Despite, the transiency of the base-pairs might decrease due to the increasing strength of the base-pairs to withstand the external force from KCl screening. The length of the sticky-ends region thus serves as another versatile tunable element, while the optimum length of the sticky ends in our system for fast aggregation is of 3-st. This fast and efficient aggregation is essential for designing bioassays for detecting DNA binding proteins that exploit the retarded aggregation due to protein stabilization of the complementary segmented dsDNA-AuNPs as demonstrated in the next section.

### Competition assay for DNA-binding protein detection and fast screening of DNA sequence selectivity using single set of segmented dsERE-AuNPs

Previously, we have demonstrated the application of the controlled assembly of segmented DNA-AuNPs conjugates for detecting dsDNA-binding protein, exemplified by the specific interaction of estrogen receptor  $\alpha$  (ER $\alpha$ ) with its cognate

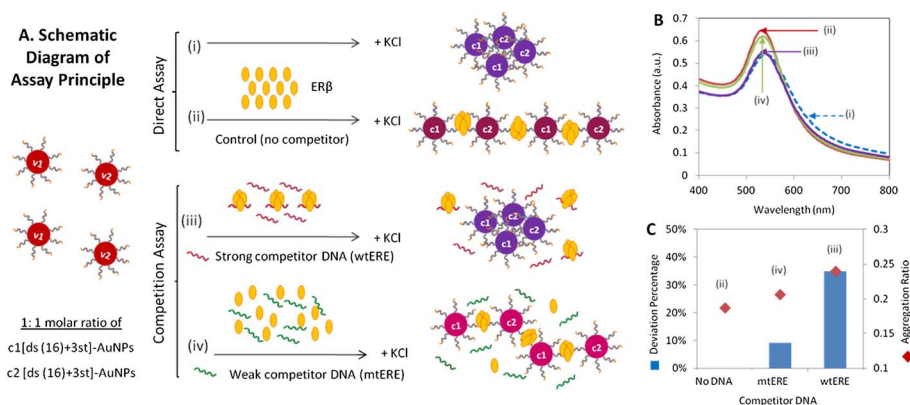


**Fig. 4** Sticky-ends effect on transient base-pairing for non-crosslinking AuNPs aggregation. UV-vis spectra and the schematic diagram (inset on top right) shows four complementary sets of segmented c1 + c2[ds(16) + (z)st]-AuNPs conjugates with a fixed length of 16 mer dsDNA spacer on each conjugate and varying number of sticky-ends, *i.e.*,  $z = 1, 3, 5$  and 8 single-base. Aggregation ratio of each sample (set A to D) is shown in the inset on left bottom.

estrogen response element (ERE).<sup>11</sup> Herein, we further validate the generality of our assay principle (see scheme I and II in Fig. 5A) for another important subtype of estrogen receptor (*i.e.*, ER $\beta$ ) with segmented perfect ERE–AuNPs conjugates. ER $\beta$  is found to have different expression pattern *in vivo* and different physiological roles from ER $\alpha$ .<sup>37</sup> recently, researchers discovered the potential of ER $\beta$  as a tumor suppressor<sup>37</sup> and sensitizers of breast cancer cells to anti-estrogenic effect of ER $\alpha$ -targeting anti-cancer drug, *i.e.*, tamoxifen.<sup>38</sup> These discoveries urge the need of high-throughput analytical methods to accelerate ER $\beta$ 's biological studies and development of personalized anti-cancer drug.<sup>39</sup>

In this study, a 35-bp dsDNA bearing the recognition ERE sequence of 5'-GGTCAnnnTGACC-3' (n: any nucleotide)<sup>40</sup> at the center was split into two segments (c1 and c2) based on the optimal DNA design of [ds(16) + 3-st]–AuNPs. Fig. 5B (curve i and ii) shows the detection of ER $\beta$  based on its stabilization effect to the complementary mixture of segmented ERE–AuNPs conjugates in salt solution from rupture by binding directly to the 'transient' full ERE sequences upon base-pairing with the short sticky-ends heading the dsDNA spacer. However, this direct binding assay is not suitable for screening large amount of protein-binding DNA sequences due to the need of cumbersome particle conjugation for each DNA. We then extended the assay into a competition approach to study sequence selectivity of ER $\beta$  to a mutant ERE sequence using the same set of complementary segmented DNA-conjugated AuNPs of the perfect ERE. In this competition assay design (see scheme iii and iv in Fig. 5A), the transient full length EREs on AuNPs upon the sticky-ends base-pairing are set to compete with free ERE competitors of different sequence and affinity, *e.g.*, mtERE (5'-GGTCAnnnTGATC-3') and the wtERE for ER $\beta$  binding. An excessive amount of unmodified DNA competitor was pre-incubated with the ER $\beta$  at room temperature for complex formation prior to the AuNPs assays (see Experimental section for details). In the presence of strong competitors (scheme 5A (iii) for wtERE), limited amount of ER $\beta$  would bind to the 'transient' ERE anchored on the AuNPs surface, leading to a

large degree of particle aggregation in salt solution. The opposite occurs with the weak competitor (scheme 5A (iv) for mtERE) that is unable to form complex with ER $\beta$  in the pre-incubation buffer. The unbound ER $\beta$  can thus bind with the ERE–AuNPs, leading to protein stabilization of AuNPs against salt-induced aggregation as observed in the direct protein–DNA binding assay. Fig. 5B (ii to iv) shows the UV-vis spectrum of the above samples with 360 nM ER $\beta$  in the absence of competitor DNA (*i.e.*, curve 5B (ii) as control) and presence of competitor DNA (*i.e.*, curve 5B (iii) for wtERE and curve 5B (iv) for mtERE). Deviation percentage defined as  $[(R_{\text{competitor}} - R_{\text{control}})/R_{\text{control}}] \times 100\%$ , is used to determine the relative binding affinity of competitor DNAs for ER $\beta$  sequence selectivity studies, based on the difference in aggregation ratio of ERE–AuNPs samples with competitors (denoted as  $R_{\text{competitor}}$ ) relative to that without competitor (denoted as  $R_{\text{control}}$ ) at 5 minutes upon mixing in the 56 mM KCl-containing protein binding buffer (Fig. 5C). AuNPs sample with the wtERE sequence as competitor recorded a deviation as high as 35.0% from the maximum stabilization exerted by the 360 nM ER $\beta$  to the system (without competitor) in 56 mM KCl solution. This deviation shows a high uptake of ER $\beta$  to form complex with the competitor wtERE sequence during incubation step, causing a large percentage of ER $\beta$  not contributing to the stabilization strength to the assembly of segmented ERE-conjugated AuNPs in salt buffer. In other words, up to 35.0% of the ER $\beta$  was not contributed to the stabilization strength to the particle aggregation while the other 65.0% was captured by the linear assembly of ERE–AuNPs conjugates. On the other hand, a 9.0% of deviation was recorded for the mtERE showing that ER $\beta$  is unable to recognize and form tight complex with the weak competitor DNA efficiently when the ERE core binding sequence is mutated. Ideally, there should be no uptake of ER $\beta$  for complex formation with this mutERE, which eases the maximum stabilization effect. Here, the deviation of up to 9.0% observed reveals the non-specific binding of ER $\beta$  to its unrecognizable dsDNA present. It has been proved that ER $\beta$  demonstrates certain degree of non-specific



**Fig. 5** (A) Assay principles for direct detection of ER $\beta$  (scheme i and ii) and competition-based sequence specificity studies (scheme iii and iv) using segmented ERE–AuNPs (B) UV-vis spectrum for the mixture of (c1 + c2)[ds(16) + 3-st]–AuNPs with 360 nM ER $\beta$  in the (ii) absence (control) and presence of competitor DNA, *i.e.*, (iii) wtERE and (iv) mtERE, at 5 minutes upon mixing in the 56 mM KCl-containing protein binding buffer. (C) Deviation percentage  $[(R_{\text{competitor}} - R_{\text{control}})/R_{\text{control}}] \times 100\%$ , calculated based on the difference in aggregation ratio (measured at  $A_{650}/A_{520}$ ) of samples with competitors relative to that without competitor to determine ER $\beta$ –DNA binding sequence selectivity.



binding under salt condition lower than 200 mM KCl measured using surface plasmon resonance spectroscopy,<sup>41</sup> as low KCl concentration is unable to effectively screen off the electrostatic interaction between the ER $\beta$  and the mtERE.

With the above experiments, we have demonstrated the utility of the as-designed segmented DNA–AuNPs conjugates for DNA-binding protein sensing as well as for fast screening of its sequence selectivity in a highly convenient competition assay format. Tedious and time-consuming conjugation of AuNPs with each tested DNA sequence can be avoided, thereby allowing direct detection of ER–DNA interactions using one set of complementary segmented ERE–AuNPs probes with various unmodified DNA.

## Conclusion

In this study, we have carried out systematic investigation on the decorating DNA design to gain better insight into the non-crosslinking AuNPs aggregation induced by the transient base-pairing and salt-charge screening for more efficient assay development. The aggregation kinetics of the segmented DNA–AuNPs conjugates are studied based on the following decorating DNA design (DNA<sub>(y+z-st)</sub>[ds(x)/ss(y – x)]–AuNPs), where  $x$  denotes the length of dsDNA portion in the composite spacer while  $y$  denotes the total length of spacer connected to a  $z$ -base sticky-ends. By tuning the structural composition of DNA spacer, dsDNA spacer of 11-bp or longer are found to be more effective than the ssDNA spacer in increasing the accessibility of short sticky-ends (*i.e.*, 3–5 bases) for immediate particle aggregation. In addition, the symmetrically spaced sticky-ends (*i.e.*,  $y_1 = y_2$ ) are found to facilitate the aggregation better than the asymmetrical combination (*i.e.*,  $y_1 \neq y_2$ ) of the complementary segmented DNA–AuNPs conjugates due to their closer initial interparticle distance. Based on the optimized assay design, we have extended its application to screen for  $\beta$  sequence selectivity in a competition arrangement with free DNA containing mutated ERE sequences. Using a single set of complementary segmented DNA–AuNPs as sensing probes, binding affinity of ER $\beta$  to different DNA sequences are detected based on the different attenuation effect to the protein stabilization against salt-induced AuNPs aggregation. This assay design offers an alternative towards simple and fast sensing of protein–DNA interactions, which could be extended to a wide range of DNA-binding molecules. With further optimization and proper DNA design, biosensing assay with high sensitivity and fast response *via* controllable AuNPs assembly would hopefully pave an alternative towards development of rapid and user-friendly test kit for field deployment.

## Experimental section

### Materials and instrumentation

Hydrogen tetrachloroaurate(III) (HAuCl<sub>4</sub>·3H<sub>2</sub>O, 99.9%) was purchased from Sigma-Aldrich. Sodium citrate dihydrate (Na<sub>3</sub>C<sub>6</sub>H<sub>5</sub>O<sub>7</sub>·2H<sub>2</sub>O, 99%) was obtained from Alfa Aesar. Purified recombinant human estrogen receptor beta (ER $\beta$ ) was supplied by PanVera Corporation (Madison, WI). Both thiolated and

unmodified DNAs used in this study (Table S1†) were synthesized by Sigma-Proligo (Singapore). All chemicals and materials were used as received without further purification. Ultrapure water (18 M $\Omega$ , prepared from Millipore Elix 3 purification system) was used as solvent unless indicated otherwise. A TECAN infinite M200 plate reader (Tecan Trading AG, Switzerland) was used to measure the UV-vis adsorption spectrum and 96 well clear flat bottom UV-transparent microplates (Corning Incorporated, USA) were used as reaction carrier. Dynamic light scattering (DLS) measurement was conducted in the Brookhaven 90PLUS nanoparticles size analyzer using 50  $\mu$ L disposable cell as the solution carrier.

### Gold nanoparticles synthesis

The 13 nm (in diameter) AuNPs were synthesized by sodium citrate reduction of HAuCl<sub>4</sub>. 5 mL sodium citrate solution (38.8 mM) was added to 45 mL boiling solution containing 1 mM HAuCl<sub>4</sub> under reflux and vigorous stirring for 15 min. The color of the solution changed from pale yellow to deep red. Stirring was continued for another 15 min after removing heating mantle and allowed to cool to room temperature for use.

### Segmented DNA–AuNPs conjugation

Segmented DNA-conjugated AuNPs (DNA<sub>(y+z-st)</sub>[ds(x)/ss(y – x)]–AuNPs), where  $y$  denotes the total length of spacer;  $x$  denotes the length of dsDNA portion and  $z$  denotes the length of sticky-ends (st) heading the dsDNA portion in the composite decorating spacer were prepared according to our previous published protocol.<sup>41</sup> In a typical conjugation, 25  $\mu$ L of the deprotected thiol-modified ssDNA (20  $\mu$ M) was added into 200  $\mu$ L of the as-synthesized AuNPs solution, and the mixture was aged for 24 h. The colloidal DNA mixture was then brought to 0.05 M NaCl in 10 mM phosphate buffer (PB) by dropwise addition of concentrated aging buffer (1 M NaCl and 0.1 M PB), and allowed to stand for 12 h, then salted to 0.1 M NaCl and aged for another 12 h. To remove excess DNA, the particle solution was centrifuged at 13 000 rpm for 15 min and the supernatant was discarded and replaced with fresh aging buffer. After three washes, the precipitated red pellet containing the ssDNA–AuNPs conjugates was redispersed in 195  $\mu$ L of DNA annealing buffer (0.1 M PBS and 0.001 M EDTA, pH 7.4), and 5  $\mu$ L of the complementary (non-thiolated) DNA (100  $\mu$ M, shorter than the sense strand to form sticky-ends) was added for hybridization. The solution was heated at 90 °C for 5 min and slowly cooled down to room temperature for 30 min. Finally, the as-prepared dsDNA–AuNPs conjugates with short sticky ends (3 to 8 bases, see Table S1† for the relevant sequences used for different studies) were re-suspended in 200  $\mu$ L of 0.1 M PBS buffer solution for use in AuNPs aggregations studies, after washing twice by centrifugation at 13 000 rpm for 15 min.

### Competition assay for ER $\beta$ binding sequence selectivity studies

Unmodified dsDNA that contains estrogen response elements (wtERE) and its mutated form (mutERE) were prepared respectively, by mixing an equal amount of the complementary



DNA strands in annealing buffer (10 mM Tris-HCl, pH 7.4, 100 mM NaCl, 1 mM EDTA). ER $\beta$  (4  $\mu$ L, 4.5  $\mu$ M) and pre-annealed unmodified dsDNA (3  $\mu$ L, 25  $\mu$ M) were pre-incubated in 280 mM KCl at room temperature for 20 min. After incubation, the complementary set of segmented ERE-conjugated c1-AuNPs and c2-AuNPs were mixed at 1 : 1 molar ratio in a solution containing the pre-incubated mixture of 360 nM ER $\beta$  and 1.5  $\mu$ M unmodified dsDNA in 56 mM KCl and 0.1 M PBS under room temperature. UV-vis spectrum of the mixture was recorded immediately and the kinetic scans were done at 1 minute interval for 10 cycles to monitor the LSPR peak shift with time.

## Acknowledgements

We would like to acknowledge the Agency for Science, Technology and Research (A\*STAR), Singapore for the financial support under the grant CCOG01\_005\_2008.

## References

- 1 R. Elghanian, J. J. Storhoff, R. C. Mucic, R. L. Letsinger and C. A. Mirkin, *Science*, 1997, **277**, 1078–1081.
- 2 W. Xu, X. Xue, T. Li, H. Zeng and X. Liu, *Angew. Chem., Int. Ed.*, 2009, **48**, 6849–6852.
- 3 Y. C. Cao, R. Jin, C. S. Thaxton and C. A. Mirkin, *Talanta*, 2005, 449–455.
- 4 W. J. Qin and L. Y. L. Yung, *Nucleic Acids Res.*, 2007, **35**, e111.
- 5 J. Liu and Y. Lu, *J. Am. Chem. Soc.*, 2007, **129**, 8634–8643.
- 6 M. S. Han, A. K. R. Lytton-Jean and C. A. Mirkin, *J. Am. Chem. Soc.*, 2006, **128**, 4954–4955.
- 7 G. Song, C. Chen, X. Qu, D. Miyoshi, J. Ren and N. Sugimoto, *Adv. Mater.*, 2008, **20**, 706–710.
- 8 J. H. Lee, Z. Wang, J. Liu and Y. Lu, *J. Am. Chem. Soc.*, 2008, **130**, 14217–14226.
- 9 X. Xue, F. Wang and X. Liu, *J. Am. Chem. Soc.*, 2008, **130**, 3244–3245.
- 10 S. J. Hurst, M. S. Han, A. K. R. Lytton-Jean and C. A. Mirkin, *Anal. Chem.*, 2007, **79**, 7201–7205.
- 11 Y. N. Tan, X. Su, Y. Zhu and J. Y. Lee, *ACS Nano*, 2010, **4**, 5101–5110.
- 12 X. Xie, W. Xu and X. Liu, *Acc. Chem. Res.*, 2012, **45**, 1511–1520.
- 13 T. Liu, J. Zhao, D. Zhang and G. Li, *Anal. Chem.*, 2010, **82**, 229–233.
- 14 X. Xu, M. S. Han and C. A. Mirkin, *Angew. Chem., Int. Ed.*, 2007, **46**, 3468–3470.
- 15 X. Xie, W. Xu, T. Li and X. Liu, *Small*, 2011, **7**, 1393–1396.
- 16 J. J. Storhoff, A. A. Lazarides, R. C. Mucic, C. A. Mirkin, R. L. Letsinger and G. C. Schatz, *J. Am. Chem. Soc.*, 2000, **122**, 4640–4650.
- 17 S.-Y. Shim, D.-K. Lim and J.-M. Nam, *Nanomedicine*, 2008, **2**, 215–232.
- 18 W. Zhao, M. A. Brook and Y. Li, *ChemBioChem*, 2008, **9**, 2363–2371.
- 19 S. Song, Y. Qin, Y. He, Q. Huang, C. Fan and H.-Y. Chen, *Chem. Soc. Rev.*, 2010, **39**, 4234–4243.
- 20 H. Pei, F. Li, Y. Wan, M. Wei, H. Liu, Y. Su, N. Chen, Q. Huang and C. Fan, *J. Am. Chem. Soc.*, 2012, **134**, 11876–11879.
- 21 K. E. Fong and L.-Y. L. Yung, *RSC Adv.*, 2013, **3**, 6076–6084.
- 22 J. J. Storhoff, R. Elghanian, C. A. Mirkin and R. L. Letsinger, *Langmuir*, 2002, **18**, 6666–6670.
- 23 S. J. Hurst, A. K. R. Lytton-Jean and C. A. Mirkin, *Anal. Chem.*, 2006, **78**, 8813.
- 24 M. M. Maye, D. Nykypanchuk, D. v. d. Lelie and O. Gang, *J. Am. Chem. Soc.*, 2006, **128**, 14020–14021.
- 25 A. P. Alivisatos, K. P. Johnsson, X. Peng, T. E. Wilson, C. J. Loweth, M. P. Bruchez Jr and P. G. Schultz, *Nature*, 1996, **382**, 609–611.
- 26 B. D. Smith, N. Dave, P.-J. J. Huang and J. Liu, *J. Phys. Chem. C*, 2011, **115**, 7851–7857.
- 27 S. Y. Park, A. K. R. Lytton-Jean, B. Lee, S. Weigand, G. C. Schatz and C. A. Mirkin, *Nature*, 2008, **451**, 553–556.
- 28 Y. Sun, N. C. Harris and C.-H. Kiang, *Physica A*, 2005, **350**, 89–94.
- 29 D. Nykypanchuk, M. M. Maye, D. v. d. Lelie and O. Gang, *Nature*, 2008, **451**, 549–552.
- 30 S. J. Hurst, H. D. Hill and C. A. Mirkin, *J. Am. Chem. Soc.*, 2008, **130**, 12192–12200.
- 31 R. J. Macfarlane, B. Lee, H. D. Hill, A. J. Senesi, S. Seifert and C. A. Mirkin, *Proc. Natl. Acad. Sci. U. S. A.*, 2009, **106**, 10493–10498.
- 32 M. M. Maye, D. Nykypanchuk, D. v. d. Lelie and O. Gang, *Small*, 2007, **3**, 1678–1682.
- 33 Y. N. Tan, K. H. Lee and X. Su, *Anal. Chem.*, 2011, **83**, 4251–4257.
- 34 Y. N. Tan, X. Su, E. T. Liu and J. S. Thomsen, *Anal. Chem.*, 2010, **82**, 2759–2765.
- 35 J. Liu and Y. Lu, *J. Am. Chem. Soc.*, 2004, **126**, 12298–12305.
- 36 M. C. Murphy, I. Rasnik, W. Cheng, T. M. Lohman and T. Ha, *Biophys. J.*, 2004, **86**, 2530–2537.
- 37 B. J. Deroo and A. V. Buensucoso, *Mol. Endocrinol.*, 2010, **24**, 1703–1714.
- 38 X. Wu, M. Subramaniam, S. B. Grygo, Z. Sun, V. Negron, W. L. Lingle, M. P. Goetz, J. N. Ingle, T. C. Spelsberg and J. R. Hawse, *Breast Cancer Res.*, 2011, **13**, R27.
- 39 S. Nilsson and J. Gustafsson, *Clin. Pharmacol. Ther.*, 2011, **89**, 44–55.
- 40 C. M. Klinge, *Nucleic Acids Res.*, 2001, **29**, 2905–2919.
- 41 H. F. Teh, W. Y. X. Peh, X. Su and J. S. Thomsen, *Biochemistry*, 2007, **46**, 2127–2135.